AGU PUBLICATIONS

Geophysical Research Letters

RESEARCH LETTER
10.1002/2016GL068468

Key Points:
- First study on potential impacts of GOES-R all-sky radiances on hurricane analysis and prediction
- Examine ensemble correlations of all-sky radiances with model state variables
- Benefits of all-sky GOES-R observations are shown for both perfect model and imperfect models

Supporting Information:
- Supporting Information S1

Correspondence to:
F. Zhang,
fzhang@psu.edu

Citation:
Zhang, F., M. Minamide, and E. E. Clothiaux (2016), Potential impacts of assimilating all-sky infrared satellite radiances from GOES-R on convection-permitting analysis and prediction of tropical cyclones, *Geophys. Res. Lett.*, *43*, doi:10.1002/2016GL068468.

Received 29 FEB 2016
Accepted 9 MAR 2016
Accepted article online 15 MAR 2016

©2016. American Geophysical Union. All Rights Reserved.

Potential impacts of assimilating all-sky infrared satellite radiances from GOES-R on convection-permitting analysis and prediction of tropical cyclones

Fuqing Zhang[1], Masashi Minamide[1], and Eugene E. Clothiaux[1]

[1]Department of Meteorology and Center for Advanced Data Assimilation and Predictability Techniques, Pennsylvania State University, University Park, Pennsylvania, USA

Abstract The potential impacts of GOES-R satellite radiances on tropical cyclone analysis and prediction were examined through ensemble correlations between simulated infrared brightness temperatures and various model state variables. The impacts of assimilating GOES-R all-sky infrared brightness temperatures on tropical cyclone analysis and prediction were further demonstrated through a series of convection-permitting observing system simulation experiments using an ensemble Kalman filter under both perfect and imperfect model scenarios. Assimilation of the high temporal and spatial resolution infrared radiances not only constrained well the thermodynamic variables, including temperature, moisture, and hydrometeors, but also considerably reduced analysis and forecast errors in the wind fields. The potential of all-sky radiances is further demonstrated through an additional proof-of-concept experiment assimilating real-data infrared brightness temperatures from GOES 13 satellite which was operational in an enhanced scanning mode during Hurricane Karl (2010).

1. Introduction

Accurate prediction of tropical cyclones can have enormous economical and societal impacts, but progress in development of more accurate predictions has so far been slow to moderate [e.g., *Cangialosi and Franklin*, 2012], especially with regard to tropical cyclone intensity, structure, and precipitation. This is at least in part due to the lack of and/or the ineffective use of high-quality, high temporal and spatial resolution observations of tropical cyclones, in particular over their inner-core areas [e.g., *Zhang et al*., 2009]. Over recent years and utilizing significant advances in computing capability, it has been demonstrated that tropical cyclone intensity and precipitation forecasts can be significantly improved through advanced assimilation of Doppler radar observations with an ensemble Kalman filter that uses flow-dependent background error covariance and a convection-permitting numerical weather prediction model [e.g., *Zhang et al*., 2009, 2011; *Aksoy et al*., 2012; *Zhang and Weng*, 2015]. Considerable forecast improvements may also be obtained through assimilation of flight level and dropsonde observations from airborne surveillance [e.g., *Wu et al*., 2010, 2014] including those from the unmanned Global Hawk aircraft [e.g., *Sippel et al*., 2013; *Munsell et al*., 2015].

Unfortunately, availability of airborne inner-core observations is limited because routine airborne Doppler radar missions are conducted only for targeted Atlantic basin storms within reach of the reconnaissance aircraft. One possible alternative to limited airborne Doppler radar data is to more effectively assimilate various satellite observations that have uninterrupted global coverage under all-sky conditions. Currently, such satellite data are grossly underutilized in high-resolution regional-scale models because of limitations in current model physics and limited capabilities in effective quality control, bias correction, and data synthesizing and thinning, which are especially challenging over cloudy and rainy areas ubiquitous to the environments of all tropical cyclones. Success in all-sky satellite data assimilation could potentially revolutionize tropical cyclone analysis and prediction, especially for tropical cyclones in regions that are hard to reach by aircraft [e.g., *Qin et al*., 2013; *Zou et al*., 2013].

Satellite observations of particular interest to this study are the brightness temperatures from geosynchronous satellites, which have (or will have) high temporal and spatial coverage of the inner-core and storm-scale structures of tropical cyclones. New satellites with high temporal and spatial resolution measurements include the Advanced Himawari Imager (AHI) on the Himawari 8 Japanese Geostationary Meteorological Satellite that was recently launched (refer to http://www.data.jma.go.jp/mscweb/technotes/msctechrep60.pdf) and the Advanced Baseline Imager (ABI) on GOES-R (refer to http://www.goes-r.gov/spacesegment/abi.html) scheduled

to be launched in 2016. Both Himawari 8 AHI and GOES-R ABI will provide higher temporal and spatial resolution data than currently available. Both ABI and AHI contain 2 visible, 4 near-infrared, and 10 infrared channels. The peaks of the clear-sky vertical weighting functions for the brightness temperatures from channels 8–10 fall in the troposphere, indicating that they are sensitive to water vapor in the upper, middle, and lower troposphere [e.g., *Otkin*, 2012, Figure 1]. The brightness temperatures from these three channels are the focus of this first proof-of-concept study. Also presented is a proof-of-concept real-data experiment assimilating all-sky infrared brightness temperatures from the existing GOES 13 satellite.

2. Forecast and Radiative Transfer Models, Data and Assimilation Methods, and Experiments

The 60-member ensemble analysis and forecast system used for this study combined the Weather Research and Forecasting (WRF, version 3.6.1) model and the ensemble Kalman filter (EnKF) developed at the Pennsylvania State University, with model domain, model physics, and ensemble configurations similar to *Zhang and Weng* [2015]. There were 60 vertical levels and 3 two-way-nested domains with horizontal grid spacings of 27 km, 9 km, and 3 km (Figure S1 in the supporting information). No cumulus scheme was used for D2 and D3.

Computations of simulated brightness temperatures were performed via the community radiative transfer model (CRTM), a rapid forward model (observation operator) for calculating satellite-based radiances [*Han et al*., 2006; *Han et al*., 2007; *Weng*, 2007]. The three water vapor channels (channels 8–10), responsive to tropospheric temperature and moisture profiles, were selected for this study. As shown in the example illustrated in Figures 1a–1c, there are strong cross correlations ($>$0.90) among the simulated brightness temperatures of these three channels over cloudy regions. We used channel 14 (11.2 μm wavelength) for subjective classification of clear-sky, cloudy-sky, and in-between conditions. These classes were subsequently used for data thinning and selecting the subsets among the three channels to be incorporated into the data assimilation for a region. Regions with brightness temperatures greater than 292 K in channel 14 were considered clear sky, in which case all three brightness temperatures from channels 8–10 were assimilated. Regions with brightness temperatures less than 285 K were treated as cloudy/rainy, in which case only brightness temperatures from channel 8 were assimilated. For channel 14 brightness temperatures from 285 K to 292 K, inclusive, only brightness temperatures from channels 8 and 10 were assimilated. Using the CRTM, synthetic observations of brightness temperatures for channels 8–10 were computed every 10 min from the reference truth simulation, each of which is then added with a random observation error with the standard deviation of 3 K.

We also assimilated tropical cyclone minimum sea level pressure (SLP) observed at the simulated center of the tropical cyclone, which is referred to as hurricane position and intensity or HPI. Hourly minimum SLP can be routinely derived from satellite images using techniques such as the Advanced Doviak Technique [*Olander and Velden*, 2007], whose accuracy is likely to be further improved with higher temporal and spatial resolution data from GOES-R. Here the minimum SLP was calculated every hour with an assumed observation error of 3 hPa.

Two perfect model observing system simulation experiments (OSSEs) were performed. The benchmark OSSE (HPI) only assimilated synthetic minimum SLP at the reference truth location every hour. Even without additional observations in the assimilation, the use of minimum SLP constrained the center of the tropical cyclone in each ensemble member close to the reference truth position. The second OSSE assimilated brightness temperatures (BTs) every 10 min in addition to the HPI every hour, hereafter referred to as the BT + HPI experiment. Both OSSEs began assimilation of synthetic observations with the cycling WRF-EnKF at 2200 UTC 16 September (hereafter 22Z/16) and continued through 00Z/18.

Because the effective horizontal resolution of the WRF-EnKF with 3 km grid spacing is much coarser than future GOES-R observations, we assimilated brightness temperatures at 12 km spacing with a 30 km radius of influence for hydrometeors and a 200 km radius of influence for other variables, including horizontal wind, temperature, pressure, mixing ratio, and dry air mass. The HPI observation was assimilated with a 300 km radius of influence. The EnKF used a relaxation coefficient of 0.5, as originally proposed in *Zhang et al*. [2004] for perfect model OSSEs.

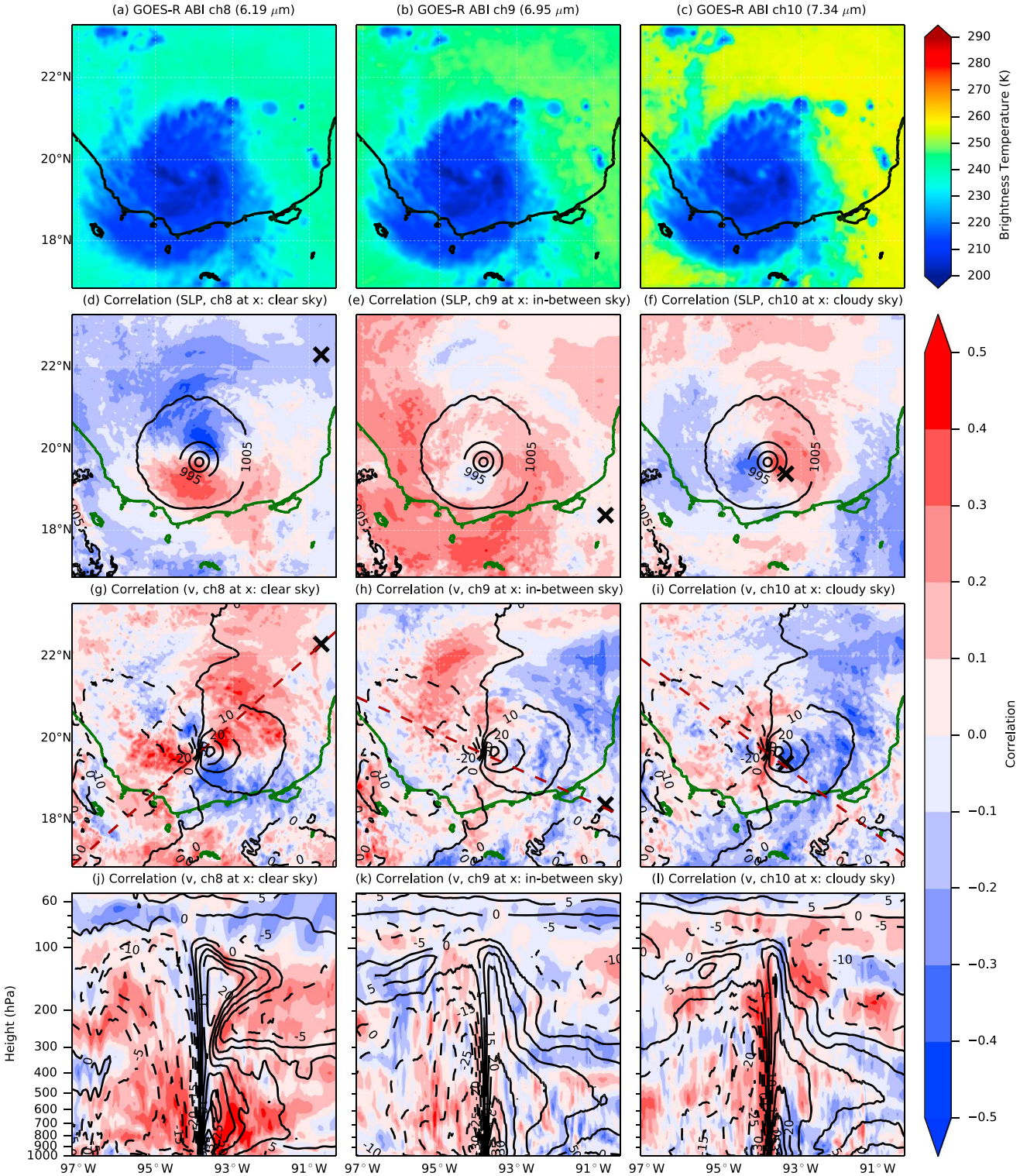

Figure 1. Simulated brightness temperatures (color shading) for GOES-R ABI (a) channel 8 (6.19 μm), (b) channel 9 (6.95 μm), and (c) channel 10 (7.34 μm). Ensemble correlations (color shading) between simulated brightness temperatures for each of the three channels at locations marked with a cross ((d) channel 8, (e) channel 9, and (f) channel 10) with sea level pressure throughout domain D3 at 23Z/16. The black contours in Figures 1d–1f represent the ensemble mean sea level pressure in 10 hPa steps. Ensemble correlations (color shading) of the three sets of ensemble channel radiances at the locations indicated in Figures 1d–1f to the (g–i) meridional winds at 930 hPa and (j–l) the meridional winds along the vertical cross sections that pass through the storm center and the channel radiance locations. The meridional winds are contoured in 10 m s^{-1} steps in Figures 1g–1i and 5 m s^{-1} steps in Figures 1j–1l.

To account for representativeness errors in assimilating satellite radiances, we adaptively estimated the observation error variance $\sigma_o^2 = \max\left\{\sigma_{ot}^2, [y_o - H(x_b)]^2 - \sigma_b^2\right\}$, where y_o represents the observations, $H(x_b)$ the simulated observations, σ_b^2 the background variance, and σ_{ot} the true observation error. Here we assumed a value of 3 K for σ_{ot}. Thus, when the innovation (observation minus the prior) was large compared to the variance of the prior estimate, the observation error was inflated; this approach served as a flow-dependent quality control method. Negative values of hydrometeor amounts in each posterior member were set to zero and positive values were proportionally adjusted to keep the ensemble mean hydrometeor amount unchanged after each EnKF analysis.

The case selected for the OSSE experiments was Hurricane Karl (2010) over the Bay of Campeche [*Sippel et al.*, 2013]. The ensemble was initialized at 12:00 UTC 16 September (12Z/16) using the NOAA's Global Forecast System (GFS) real-time analyses and forecasts for initial and boundary conditions. The WRF-EnKF assimilated airborne Doppler radar measurements from the NOAA P3 aircraft at 19Z/16, 20Z/16, and 21Z/16 as in *Zhang and Weng* [2015]. The EnKF analysis and perturbations at 21Z/16 were used to initialize 61 free-running WRF forecasts until 00Z/18. The ensemble member with the second lowest minimum sea level pressure at 00Z/17 was used as the reference truth run. This truth run was used both to generate observations and to validate the performances of the EnKF analyses and forecasts. The other ensemble members were used as perturbed initial conditions for the OSSEs.

3. Potential Impacts of Brightness Temperatures Revealed From Ensemble Correlations

We first explore the potential impacts of brightness temperatures (BTs) through examining the structure and dynamics of the correlations between the clear- and cloudy-sky BTs and the model state variables through convection-allowing ensemble simulations and CRTM calculations. The CRTM-simulated ensemble mean BTs from channels 8–10 (Figures 1a–1c), labeled henceforth as ch8, ch9, and ch10, clearly show the impact of the tropical cyclone on them with lower BTs for all three channels over the primary eyewall and outer rainbands but much higher BTs over the clear-sky areas outside the storm. We select ensemble brightness temperatures for clear-sky conditions (BT1 from ch8 at −90.72°W, 22.27°N, Figure 1d), in-between conditions (BT2 from ch9 at −90.72°W, 18.34°N, Figure 1e), and cloudy-sky conditions (BT3 from ch10 at −93.42°W, 19.36°N, Figure 1f) to illustrate the correlations between them and several state variables across domain D3. The moderate to strong ensemble correlations between SLP and BT in each panel (Figures 1d–1f) suggest the potential value of assimilating infrared BTs under all-sky conditions to improve the analysis of tropical cyclone intensity and structure. For example, the correlation pattern in Figure 1d suggests warmer (colder) BT1 will correspond to lower (higher) SLP to the north of the mean center and higher (lower) SLP to the south of the storm center. The pattern in Figure 1e suggests that warmer (colder) BT2 in this in-between location implies lower (higher) overall SLP. Warmer (colder) BT3 in the eyewall implies weaker (stronger) convection at this location, but the correlations with SLP are highly variable across the domain (Figure 1f). The potential impacts of assimilating these BTs are further exemplified in the correlations of these three sets of BTs with the *v* (meridional) wind both at 930 hPa (Figures 1g–1i) and along the vertical cross sections (illustrated in Figures 1g–1i) that pass through the storm center and the radiance locations (Figures 1j–1l). For example, warmer (colder) BT1 corresponds to larger (smaller) *v* wind to the northeast and southwest (northwest and southeast) of the storm center. Thus, the cyclonic flow of the storm is stronger (weaker) to the north (south) of the storm center. Figures 1j–1l shows that the large impact is likely to be in the lower troposphere where the horizontal winds are strong but the correlations (hence potential impacts) are widely distributed throughout the troposphere.

Comparable or even stronger ensemble correlations exist between the BTs and the temperature and moisture fields (not shown) because temperature and moisture are what the BTs directly respond to. These correlation analyses point to the potential impacts of BT assimilation on tropical cyclone analysis and prediction that will be further illustrated through assimilation of synthetic GOES-R BTs below.

4. Proof-of-Concept Perfect Model OSSE for Assimilating BTs From GOES-R

We first compare the EnKF analyses between the two OSSEs, progressing from HPI to BT + HPI to demonstrate the potential impacts of future GOES-R satellite observations on tropical cyclone analysis and forecasting.

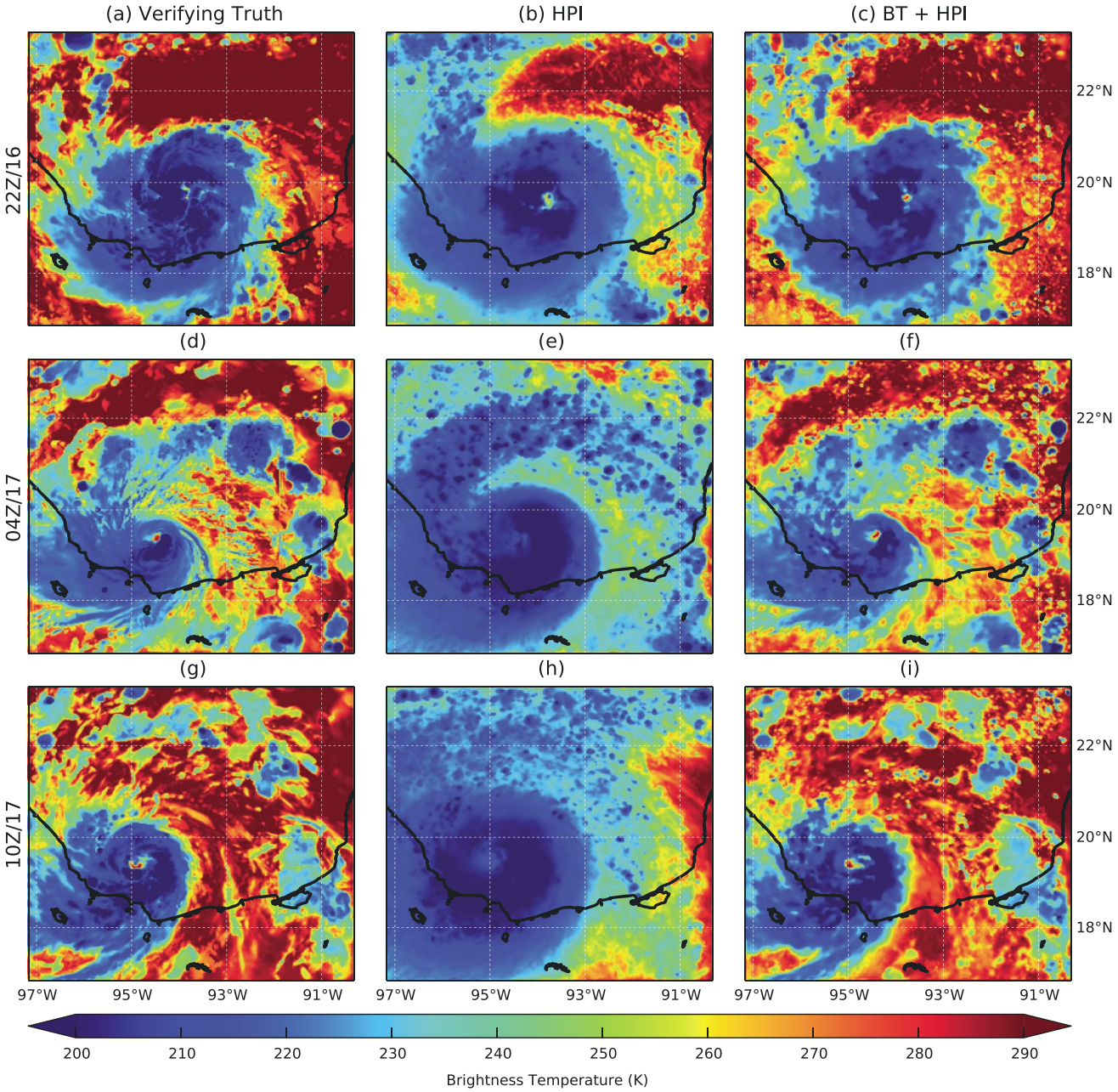

Figure 2. Simulated brightness temperatures (color shading) of GOES-R ABI channel 14 at (a–c) 22Z/16, (d–f) 04Z/17, and (g–i) 10Z/17 from the (Figures 2a, 2d, and 2g) verifying truth, (Figures 2b, 2e, and 2h) HPI OSSE, and (Figures 2c, 2f, and 2i) BT + HPI OSSE.

Figure 2 shows comparisons of the EnKF analyses of simulated ch14 (11.2 μm) BTs at 22Z/16, 04Z/17, and 10Z/17 (i.e., 0 h, 6 h, and 12 h after the initial assimilation begins) between the verifying truth and both OSSEs (with differences between verifying truth shown in Figure S2**).** (Note that ch14 is sensitive to particulates—clouds and the surface—but was not assimilated.) Figure S3 shows comparisons of simulated SLP and the column-maximum radar reflectivity, which are representative of tropical cyclone intensity and structure. An animation of the EnKF analyses versus the verifying truth is available at the website http://hfip.psu.edu/mum373/anim_bt.gif.

After the first EnKF assimilation at 22Z/16, the BT + HPI analysis is able to approximate not only the patterns in the simulated ch14 BTs associated with the eyewall and primary rainbands but also some small-scale convective clouds among the clear-sky regions, all of which are considerably better than for the HPI experiment assimilating only minimum SLP (Figures 2a–2c). These improvements are reflected in the EnKF-simulated

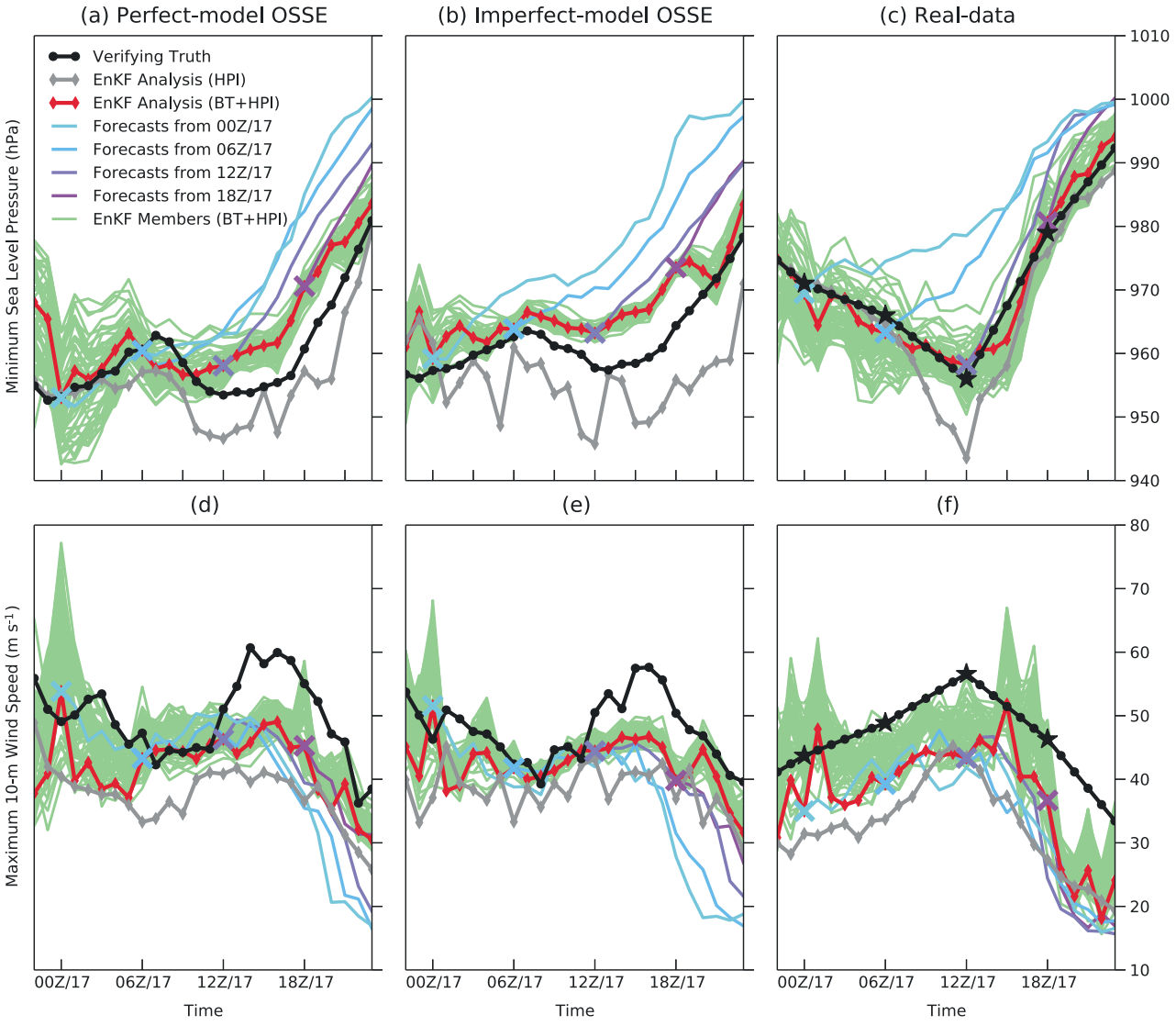

Figure 3. Time evolution of tropical cyclone intensity in terms of (a–c) minimum sea level pressure (hPa) and (d–f) maximum 10 m wind speed ($m\,s^{-1}$) for the verifying truth and different OSSE EnKF analyses and forecasts (color coded). Results for the (Figures 3a and 3d) perfect model, (Figures 3b and 3e) imperfect model, and (Figures 3c and 3f) real-data assimilation experiments are illustrated.

radar reflectivity, which is more sensitive to the content of the hydrometers, though the improvement over the HPI experiment is not as impressive after the first EnKF analysis cycle (Figures S3a–S3c). The BT + HPI assimilation also improves considerably the structure and intensity of the 10 m wind field, though mostly in the inner-core area and immediate surroundings (not shown).

Continuous BT + HPI assimilation for 6 h and 12 h further improves the analyzed BTs of ch14 in terms of both accuracy and cloud pattern/content with increasingly finer-scale individual convective clouds embedded in the clear-sky area and amid the inner core of the hurricane eye (Figures 2d, 2f, 2g, and 2i). The EnKF analysis for the HPI OSSE, while maintaining a tropical cyclone structure, has an overly extensive cloud field with a nearly complete loss of smaller-scale features (Figures 2e and 2h). The HPI OSSE does not lead to a noticeable clear-sky area within the eyewall (Figures 2e and 2h), whereas the BT + HPI OSSE does (Figures 2f and 2i). The advantages of assimilating brightness temperatures can also be seen in changes in three-dimensional meridional winds (not shown) that are consistent with the ensemble correlations shown in Figure 1.

Given the significance of the maximum 10 m wind speed and minimum SLP in operational tropical cyclone forecasting, Figure 3 shows the comparison of these two quantities between the verifying truth (black)

and the analyses from both OSSEs. Also shown in Figure 3 are the uncertainties and deficiencies in the EnKF analyses in the BT + HPI OSSE, represented by the maximum 10 m wind and minimum SLP in each of the analysis ensemble members. Likely the result of the extensive, but smoothed, cloud fields, the HPI OSSE analyzed minimum SLP is considerably deeper than the others (gray versus dark curves in Figure 3a). However, the analyzed maximum 10 m wind speed is considerably weaker than the verifying truth (Figure 3d) and the BT + HPI OSSE throughout the assimilation period, especially during stages of peak intensity.

After a couple of hours of initial adjustments, additional assimilation of BTs in the BT + HPI OSSE (red curves in Figures 3a and 3d) improves the intensity analysis, though the minimum SLP is still too high relative to the reference truth during the stages of peak intensity. This is likely due to an increasingly smaller ensemble spread at this stage, suggesting that the EnKF analysis might have some local filter divergence. This issue will be addressed in future studies through sensitivity tests of filter configurations, including but not limited to covariance inflation and localization.

Also shown in Figures 3a and 3d are the deterministic forecasts initialized with the mean EnKF analysis from the BT + HPI OSSE at a few selected times (00Z, 06Z, 12Z, and 18Z/17). These deterministic forecasts are used to assess the impact of BT assimilation on the intensity forecast. Not unexpectedly, deterministic forecasts initialized with the BT + HPI analyses become increasingly more accurate with both decreasing lead times and more assimilated satellite data.

5. Proof-of-Concept Imperfect Model OSSE for Assimilating BTs From GOES-R

The reference truth and ensemble simulations for the EnKF analysis in the previous section used exactly the same WRF model configuration without consideration of model uncertainties, which are often referred to as perfect model ("identical twin") OSSEs. Because there are considerable model errors and uncertainties in tropical cyclone prediction [e.g., *Green and Zhang*, 2013], we conducted a second proof-of-concept BT + HPI experiment. This second experiment maintained its configuration from the prior OSSE experiment, but the reference truth (and thus the observations) was also produced by the WRF model but with different model physics. We used the Ferrier microphysics scheme [*Rogers et al*., 2001] and the Geophysical Fluid Dynamics Laboratory longwave and shortwave radiation schemes [*Fels and Schwarzkopf*, 1981] for the truth run of the imperfect model OSSE to represent realistic, large model error. For the perfect model OSSE truth run and ensemble, we used the WRF single-moment six-class mixed-phase microphysics scheme [*Hong and Lim*, 2006] and the rapid radiative transfer model longwave and shortwave radiation schemes [*Iacono et al*., 2008].

Although the new reference truth run has similar intensities (Figures 3b and 3e versus Figures 3a and 3d) to that in the perfect model OSSEs of the previous section, there are considerable differences in the cloud patterns, in particular the structure of the primary rainband and outer-core peripheral convection (Figures 4a, 4e, and 4i versus Figures 2a, 2d, and 2g). The EnKF analysis for the BT + HPI OSSE in the imperfect model experiment performs nearly as well (Figures 3b, 3e, and 4) as the perfect model BT + HPI OSSE presented in the previous section (Figures 2, 3a, and 3d). The differences between verifying truth/observation and EnKF analysis of Figure 4 are shown in Figure S4.

Further evidence of resilience in the WRF-EnKF assimilation of BTs with an imperfect model is seen in the verification of radar reflectivity (SF5). Although future research is necessary to understand the extent of model error and uncertainty impacts on tropical cyclone analysis and prediction, this imperfect model OSSE further supports the potential beneficial impacts of assimilating future GOES-R observations.

6. Proof-of-Concept Real-Data Experiment Assimilating BTs From GOES 13

To demonstrate the relevance of the OSSE results presented above to real-data situations, we performed an additional IR radiance assimilation experiment using exactly the same forecast model, initial ensemble perturbations, and EnKF configuration as for the OSSEs but with assimilation of real-data channel 3 (ch3, or the 6.5 μm water vapor channel) IR radiances from the existing GOES 13 satellite which was operational during Hurricane Karl (2010). The International Best Track Archive for Climate Stewardship [*Knapp et al*., 2010] minimum SLP estimates linearly interpolated to every 1 h interval were assimilated as HPI observations. The GOES 13 was operated in an experimentally enhanced scanning mode available every 15 min, and at

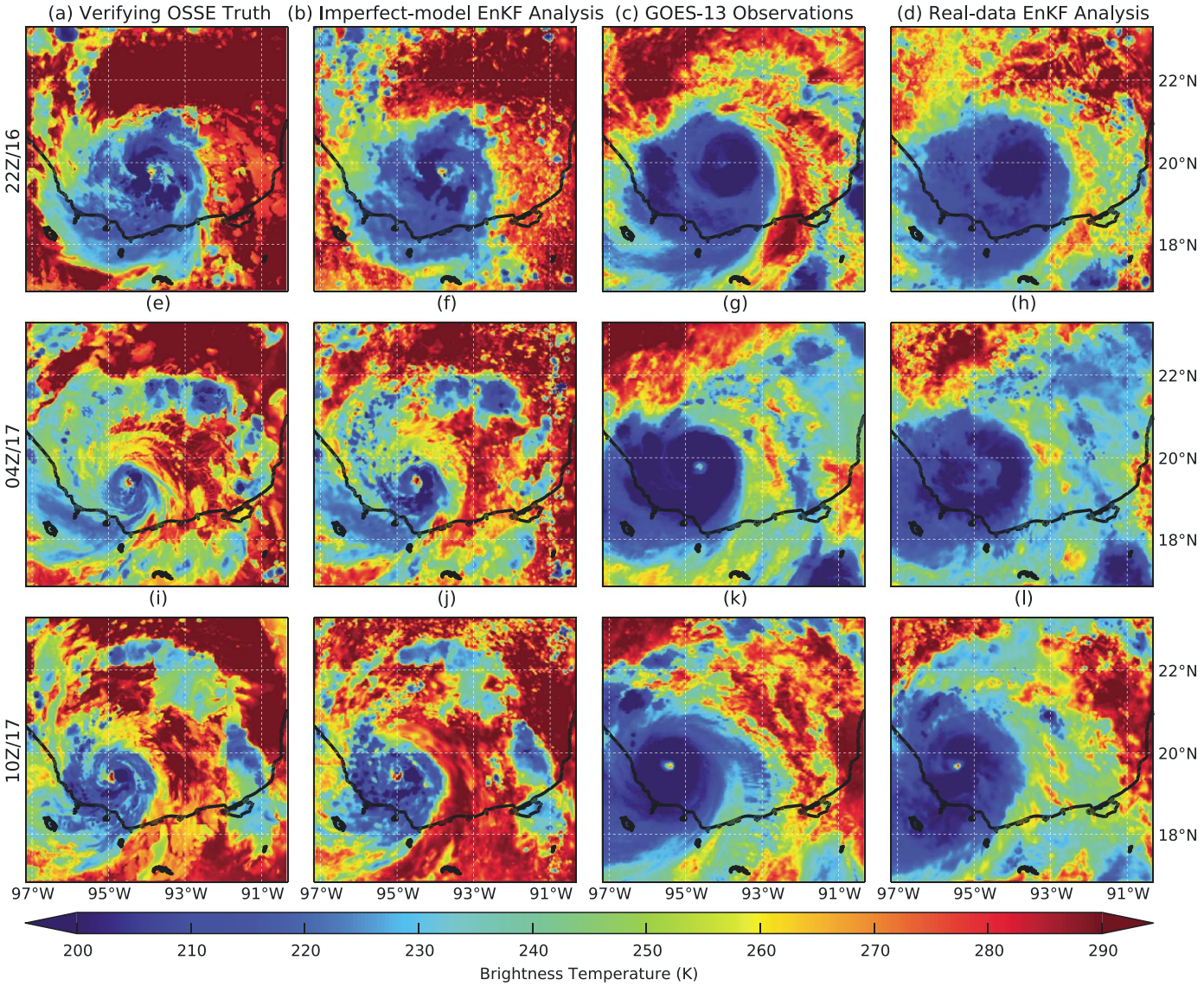

Figure 4. As in Figure 2 but for GOES-R ABI channel 14 from the imperfect model BT + HPI OSSE (Figures 4a, 4b, 4e, 4f, 4i, and 4j) and GOES-13 channel 4 from the real-data assimilation (Figures 4c, 4d, 4g, 4h, 4k, and 4l).

approximately 4 km horizontal resolution, the real-data all-sky channel 3 infrared brightness temperatures were first interpolated to the 3 km WRF domain 3 but were subsequently assimilated in a reduced density the same as in the OSSEs. The same observation errors were assigned to the HPI and brightness temperature observations as in the OSSEs as well.

Despite the fact that the EnKF assimilation of GOES 13 channel 3 IR radiances was possible only every 15 min, representing a lower effective observation density compared to the OSSEs that represent the future GOES-R, and despite the fact that there were more error sources involved, results of the real-data experiment assimilating GOES 13 channel 3 radiances are also very encouraging. The right two columns of Figures 4 and S4 show the verification of the real-data EnKF analyses against the independent brightness temperature observations from GOES 13 channel 4 (ch4, 10.2 μm; not assimilated). The real-data WRF-EnKF analyses and forecasts of Karl's intensity in terms of both minimum sea level pressure and maximum surface wind speed are shown in Figures 3c and 3f. For the most part, the real-data proof-of-concept experiment is consistent with the OSSE experiments presented in previous sections. Although assimilation of all-sky satellite infrared observations in cloudy regions of tropical cyclones is undoubtedly challenging, this real-data proof-of-concept experiment suggests that the associated uncertainties do not cancel the benefits that are shown in the OSSEs.

7. Concluding Remarks

The potential importance of future GOES-R satellite radiances under all-sky conditions in tropical cyclone analysis and prediction is first revealed through systematic examination of the ensemble correlations between simulated infrared brightness temperatures of GOES-R channels 8–10 and various model state variables. The potential impacts of assimilating all-sky infrared brightness temperatures for tropical cyclone analysis and prediction are further demonstrated through a series of convection-permitting observing system simulation experiments using an ensemble Kalman filter under both perfect and imperfect model scenarios using a combination of existing and newly proposed methodologies, such as channel selection, adaptive observation errors, and control of negative hydrometeor amounts. Assimilation of the high temporal/spatial resolution all-sky infrared radiances not only constrained well-analyzed thermodynamic variables, including temperature, moisture, and hydrometeors, but also considerably reduced the analysis and forecast errors in the wind and sea level pressure fields. Although slightly less accurate, a second proof-of-concept OSSE experiment using the WRF-EnKF system with an imperfect model also led to improvements under all-sky conditions despite considerable differences (errors) in the model physics used to represent cloud and radiation parameterizations between the truth run and the OSSE ensemble. The potential of all-sky radiances is further demonstrated through a real-data experiment assimilating infrared brightness temperatures from channel 3 (6.5 μm) of the existing GOES 13 satellite which was operational in an enhanced scanning mode during Hurricane Karl (2010), whose performance is for the most part consistent with the OSSE experiments.

However, this first proof-of-concept study did not consider many other challenges in assimilating future GOES-R all-sky radiances. These challenges include, but are not limited to, systematic errors and biases in both the instrument and CRTM, more complex model errors, radiances collected at different scan angles, correlated observations, data thinning, and quality control. Moreover, the EnKF configurations used in this study were by no means optimal. These issues must be considered in subsequent studies and within the context of more systematic real-data experiments. Nevertheless, our experiments demonstrate that there are apparent zeroth-order benefits to be obtained from assimilation of cloudy radiances for tropical cyclone analysis and prediction despite model or data assimilation deficiencies.

Acknowledgments

This research is partially supported by NSF grant 1305798, ONR grant N000140910526, and NASA grant NNX12AJ79G. M.M. was supported by Japan's Funai Overseas Scholarship of the Funai Foundation for Information Technology. Discussions and technical support from Yue (Michael) Ying, Yonghui Weng, Christopher Melhauser, Jason Otkin and Scott Sieron are greatly appreciated. Comments by two anonymous reviewers are very beneficial. Computing was provided by the Texas Advanced Computing Center. All data presented are stored and can be accessed through the TACC data archive.

References

Aksoy, A., S. Lorsolo, T. Vukicevic, K. J. Sellwood, S. D. Aberson, and F. Zhang (2012), The HWRF Hurricane Ensemble Data Assimilation System (HEDAS) for high-resolution data: The impact of airborne Doppler radar observations in an OSSE, *Mon. Weather Rev.*, *140*, 1843–1862.

Cangialosi, J. P., and J. L. Franklin (2012), National Hurricane Center verification report Tropical Prediction Center, National Hurricane Center, National Center for Environmental Prediction, National Weather Center, NOAA, 76 pp.

Fels, S. B., and M. D. Schwarzkopf (1981), An efficient, accurate algorithm for calculating CO_2 15 μm band cooling rates, *J. Geophys. Res.*, *86*, 1205–1232, doi:10.1029/JC086iC02p01205.

Green, B. W., and F. Zhang (2013), Impacts of air–sea flux parameterizations on the intensity and structure of tropical cyclones, *Mon. Weather Rev.*, *141*, 2308–2324.

Han, Y., P. V. Delst, Q. Liu, F. Weng, B. Yan, R. Treadon, and J. Derber (2006), NOAA Techn. Rep. NESDIS 122 JCSDA community radiative transfer model (CRTM)—Version 1 NOAA Tech. Rep., (August).

Han, Y., F. Weng, Q. Liu, and P. V. Delst (2007), A fast radiative transfer model for SSMIS upper atmosphere sounding channels, *J. Geophys. Res.*, *112*, D11121, doi:10.1029/2006JD008208.

Hong, S., and J. Lim (2006), The WRF single-moment 6-class microphysics scheme (WSM6), *J. Korean Meteorol. Soc.*, *42*, 129–151.

Iacono, M. J., J. S. Delamere, E. J. Mlawer, M. W. Shephard, S. A. Clough, and W. D. Collins (2008), Radiative forcing by long-lived greenhouse gases: Calculations with the AER radiative transfer models, *J. Geophys. Res.*, *113*, D13103, doi:10.1029/2008JD009944.

Knapp, K. R., M. C. Kruk, D. H. Levinson, J. H. Diamond, and J. C. Neumann (2010), The International Best Track Archive for Climate Stewardship (IBTrACS) unifying tropical cyclone data, *Bull. Am. Meteorol. Soc.*, *91*, 363–376.

Munsell, E. B., J. A. Sippel, S. A. Braun, F. Weng, and F. Zhang (2015), Dynamics and predictability of Hurricane Nadine (2012) evaluated through convection-permitting ensemble analysis and forecasts, *Mon. Weather Rev.*, *143*, 4514–4532.

Olander, T. L., and C. S. Velden (2007), The advanced Dvorak technique: Continued development of an objective scheme to estimate tropical cyclone intensity using geostationary infrared satellite imagery, *Weather Forecast.*, *22*, 287–298.

Otkin, J. (2012), Assimilation of water vapor sensitive infrared brightness temperature observations during a high impact weather event, *J. Geophys. Res.*, *117*, D19203, doi:10.1029/2012JD017568.

Qin, Z., X. Zou, and F. Weng (2013), Evaluating added benefits of assimilating GOES imager radiance data in GSI for coastal QPFs, *Mon. Weather Rev.*, *141*, 75–92.

Rogers, E., Black T., Ferrier B., Lin Y., Parrish D., and DiMego G. (2001), NCEP Meso Eta Analysis and Forecast System: Increase in resolution, new cloud microphysics, modified precipitation assimilation, modified 3DVAR analysis, *NWS Techn. Proced. Bull.*, *488*, 1–15. [Available at http://www.emc.ncep.noaa.gov/mmb/mmbpll/eta12tpb/.]

Sippel, J. A., S. A. Braun, F. Zhang, and Y. Weng (2013), Ensemble Kalman filter assimilation of simulated HIWRAP Doppler velocity data in a hurricane, *Mon. Weather Rev.*, *141*, 2683–2704.

Weng, F. (2007), Advances in radiative transfer modeling in support of satellite data assimilation, *J. Atmos. Sci.*, *64*(11), 3799–3807.

Wu, C.-C., G.-Y. Lien, J.-H. Chen, and F. Zhang (2010), Assimilation of tropical cyclone track and structure based on the ensemble Kalman filter (EnKF), *J. Atmos. Sci.*, *67*, 3806–3822.

Wu, T.-C., H. Liu, S. J. Majumdar, C. S. Velden, and J. L. Anderson (2014), Influence of assimilating satellite-derived atmospheric motion vector observations on numerical analyses and forecasts of tropical cyclone track and intensity, *Mon. Weather Rev.*, *142*, 49–71.

Zhang, F., and Y. Weng (2015), Predicting hurricane intensity and associated hazards: A five-year real-time forecast experiment with assimilation of airborne Doppler radar observations, *Bull. Am. Meteorol. Soc.*, *96*, 25–33.

Zhang, F., C. Snyder, and J. Sun (2004), Impacts of initial estimate and observation availability on convective-scale data assimilation with an ensemble Kalman filter, *Mon. Weather Rev.*, *132*, 1238–1253.

Zhang, F., Y. Weng, J. A. Sippel, Z. Meng, and C. H. Bishop (2009), Cloud-resolving hurricane initialization and prediction through assimilation of Doppler radar observations with an ensemble Kalman filter, *Mon. Weather Rev.*, *137*, 2105–2125.

Zhang, F., Y. Weng, J. F. Gamache, and F. D. Marks (2011), Performance of convection-permitting hurricane initialization and prediction during 2008–2010 with ensemble data assimilation of inner-core airborne Doppler radar observations, *Geophys. Res. Lett.*, *38*, L15810, doi:10.1029/2011GL048469.

Zou, X., F. Weng, B. Zhang, L. Lin, Z. Qin, and V. Tallapragada (2013), Impacts of assimilation of ATMS data in HWRF on track and intensity forecasts of 2012 four landfall hurricanes, *J. Geophys. Res. Atmos.*, *118*, 11,558–11,576.